Chemical Engineering Journal 334 (2018) 638–649

Contents lists available at ScienceDirect

Chemical Engineering Journal

journal homepage: www.elsevier.com/locate/cej

Settleable engineered titanium dioxide nanomaterials for the removal of natural organic matter from drinking water

Stephanie Gora[a,*], Robert Liang[b], Y. Norman Zhou[b], Susan Andrews[a]

[a] Department of Civil Engineering, University of Toronto, 35 St. George Street, Toronto, Ontario M5S 1A4, Canada
[b] Department of Mechanical and Mechatronics Engineering, University of Waterloo, 200 University Avenue West, Waterloo, Ontario N2L 3G1, Canada

ARTICLE INFO

Keywords:
Titanium dioxide
Engineered nanomaterials
Photocatalysis
Settling
Natural organic matter

ABSTRACT

Four linear engineered TiO_2 nanomaterials (LENs) were synthesized and evaluated in terms of settlability and their ability to remove natural organic matter (NOM) from river water. The size, surface characteristics, and crystallinity of the LENs were manipulated by varying the temperatures used during the synthesis procedure. All four LENs settled out of purified water more effectively than standard Degussa Evonik Aeroxide P25 nanoparticles. The settling behaviour of the nanomaterials was impacted by surface charge effects and interactions with NOM and ionic species in the river water matrix. The reduction of two disinfection byproduct precursor surrogate parameters, DOC and UV254, by the LENs via adsorption (no irradiation) and photocatalytic degradation under UVA LED irradiation was compared to that by P25 nanoparticles. After 60 min of irradiation DOC removal by the LENs ranged from 20 to 50% and UV254 reduction ranged from 65 to 90%. Two of the most promising LENs were reused multiple times and although both materials experienced decreases in treatment efficacy over successive reuse cycles, the reusability of both LENs was equal to or superior to that of P25 nanoparticles. The electrical energy per order required to remove DOC and UV254 from the water ranged from 8 to 36 times higher than that required for UV/H_2O_2 treatment but comparable to results reported by other researchers using UV/TiO_2 for NOM removal. A subset of the nanomaterials evaluated in this study may prove to be a viable alternative to standard TiO_2 nanoparticles for the removal of DBP precursors from drinking water, but the characteristics of the water matrix have important effects on settling efficiency and will require site-specific evaluation.

1. Introduction

Oxidation processes, including advanced oxidation processes (AOPs) that combine two or more existing treatment technologies to enhance the removal of hazardous and/or recalcitrant to removal via traditional methods, have become a mainstay of modern drinking water treatment. TiO_2 photocatalysis (UV/TiO_2), which combines a nanoscale semiconductor photocatalyst with UV light, is an emerging AOP that may one day prove to be a useful addition to the existing suite of oxidation processes. When irradiated with UV light at or below 385 nm TiO_2 catalyzes the formation of reactive oxygen species (ROS), including hydroxyl radicals, as well as photogenerated electron holes, which are also highly oxidative. These species can degrade organic contaminants adsorbed to the surface of the TiO_2 nanoparticle [1]. In the laboratory, TiO_2 photocatalysis has been used to destroy numerous water contaminants including various types of bacteria [2], taste and odour compounds [3] natural organic matter (NOM) [4,5], and various anthropogenic contaminants [6,7].

Despite the promise that TiO_2 holds for drinking water and wastewater treatment, it has yet to be widely adopted for these purposes, mostly because it has proven difficult to design a reactor that is simultaneously capable of ensuring adequate treatment efficiency while also working within the practical confines of a water treatment plant. The need to remove the TiO_2 from the water after treatment is also a major concern because TiO_2 nanomaterials are themselves potentially hazardous to human health [8] and the environment [9]. Some researchers have attempted to address this by immobilizing TiO_2 on solid supports. Examples include nanoparticles attached to or integrated into magnetized particles [10,11], glass beads [12,13], and zeolites [14]. In this study, we prepared and investigated the use of pure TiO_2 (non-immobilized) settleable linear engineered nanomaterials (LENs)

Abbreviations: AOP, advanced oxidation process; DBP, disinfection byproduct; DBPfp, disinfection byproduct formation potential; DOC, dissolved organic carbon; EEO, electrical energy per order; HAA, haloacetic acid; IEP, isoelectric point; LED, light emitting diode; LEN, linear engineered nanomaterial; NB, nanobelt; NOM, natural organic matter; ROS, reactive oxygen species; SUVA, specific UV absorbance; THM, trihalomethane; TOC, total organic carbon; UV254, absorbance at 254 nm

* Corresponding author.
E-mail addresses: stephanie.gora@mail.utoronto.ca (S. Gora), rliang@uwaterloo.ca (R. Liang), nzhou@uwaterloo.ca (Y.N. Zhou), sandrews@civ.utoronto.ca (S. Andrews).

http://dx.doi.org/10.1016/j.cej.2017.10.058
Received 25 July 2017; Received in revised form 12 September 2017; Accepted 13 October 2017
Available online 16 October 2017
1385-8947/

synthesized from the most commonly available form of laboratory grade TiO_2, Degussa Evonik Aeroxide P25 nanoparticles, for the treatment of drinking water.

The alkaline hydrothermal method used to synthesize these materials was first described by Kasuga et al. [15] and is by now so widely known that it can be found in the public domain. A precursor compound (usually P25 nanoparticles or anatase nanoparticles) is suspended in alkaline solution and heated above 100 °C for a period of time ranging from 20 h to 4 days. The resulting material, which consists of sodium disodium trititanate ($Na_2Ti_3O_7$), is then washed with acid and water to remove the Na^+ ions and then calcined at temperatures ranging from 300 °C to 900 °C to yield a final product consisting of $H_2Ti_3O_7$, TiO_2 (anatase or rutile), or other crystalline structures depending on the temperature used. The linear materials formed at the end of this process are tubular or belt like with diameters in the nanoscale range and lengths in the nanoscale or microscale range. Although many researchers have employed some version of this process to yield linear nanomaterials, their results are difficult to compare to one another because the researchers have employed different synthesis regimes and there remains some debate as to the individual impacts of the many steps of the procedure on the final product [16]. In the present study, we employed a set of synthesis regimes informed by the findings of Yuan and Su [17], Qamar et al. [18], and Zheng et al. [19] that we predicted would retain or enhance the photoactivity and/or settleability of the nanomaterials.

NOM is a blanket term that encompasses an array of organic carbon compounds that are formed through the degradation of organisms and their detritus in the natural environment. It is commonly quantified as total organic carbon (TOC), dissolved organic carbon (DOC), or based on its ability to absorb UV light at various wavelengths, including 254 nm (UV254). NOM has a number of undesirable aesthetic, operational, and health effects on drinking water, and its removal is one of the primary goals in many water treatment plants. Most importantly, the interaction of NOM with chemical treatment processes can result in the formation of undesirable reaction products, including disinfection byproducts (DBPs). Certain classes of DBPs, usually trihalomethanes (THMs) and haloacetic acids (HAAs), are regulated in most jurisdictions in North America. Although recent research has revealed that negative health effects are unlikely to occur in humans exposed to the concentrations of THMs and HAAs commonly found in drinking water [20], they continue to be regulated, partly because they represent only a small subset of the DBPs formed when NOM reacts with chemical disinfectants such as chlorine and monochloramine. Almost all of these are currently unregulated but there is evidence that some may be more toxic than the DBPs that are currently regulated [21]. For example, the formation of halogenated furanones such as Mutagen X (MX), a highly genotoxic DBP, has been shown to be correlated to the formation of HAAs [22]. DOC and UV254 are widely used as surrogate parameters for DBP precursors because they are simple to measure and well correlated with THM and HAA [23,24]. They have also been shown to be correlated to MX formation in some water sources [22].

NOM, including the precursors of regulated and unregulated DBPs, can be removed using existing water treatment processes such as coagulation but there is demand for alternative NOM removal processes that are less chemically intensive and produce less waste. The aim of this research was to evaluate the impact of different steps of the hydrothermal synthesis method on the settleability of four new and potentially reusable photocatalytic TiO_2 nanomaterials and their ability to adsorb and photocatalytically degrade NOM and DBP precursors as quantified using DOC and UV254. One of these materials was selected for further assessment and evaluated in terms of its ability to remove THM and HAA precursors. To the authors' knowledge, no other research groups have explored the application of LENs for NOM removal in real drinking water matrices, the impacts of the hydrothermal and calcination temperature on the ability of TiO_2 LENs to remove NOM, or the use of sedimentation as a post treatment separation step.

Table 1
Summary of raw water quality.

Parameter	Units	Value
DOC	mg/L	4.6 ± 0.3[1]
UV254	1/cm	0.12 ± 0.01[1]
Specific UV Absorbance (SUVA)	m/mg.L	2.7 ± 0.2[1]
pH		8.2 ± 0.2[2]
Turbidity	NTU	0.6 ± 0.2[2]
Alkalinity	mg/L as $CaCO_3$	87 ± 7[2]
Hardness	mg/L as $CaCO_3$	95 ± 11[2]
Calcium	mg/L	32.8 ± 3.7[2]
Magnesium	mg/L	3.2 ± 0.3[2]
Sodium	mg/L	6.5 ± 0.8[2]
Chloride	mg/L	11.5 ± 1.3[2]
Conductivity	µS/cm	214 ± 19[2]

[1] Average and standard deviation of samples.
[2] Average and standard deviation of values obtained from Ontario Drinking Water Surveillance Program 2010–2012.

2. Experimental

2.1. Materials

Degussa Evonik Aeroxide P25 TiO_2 nanoparticles were obtained from Sigma Aldrich and used as the precursor material for the four engineered nanomaterials. They were also used in unmodified form as a reference material during the degradation experiments and the settling tests. Raw water was obtained from the inlet of the Peterborough water treatment plant in Ontario, Canada, which treats water from the Otonabee River. The Otonabee River is typical of many smaller surface water sources in southern Ontario in that it has moderate levels of NOM and alkalinity, low turbidity, and pH above neutral. Table 1 contains a summary of relevant water quality parameters in the raw water.

2.2. Synthesis of engineered nanomaterials

Four engineered TiO_2 nanomaterials were synthesized via a basic hydrothermal as described by numerous researchers [15,17–20] to create tubular or belt-like engineered TiO_2 nanomaterials. Two grams of P25 nanoparticles were added to a Teflon-lined reactor along with 60 mL of a 10 N NaOH and mixed vigorously using a glass rod. The Teflon-lined reactor was placed in a muffle furnace and heated to 130 °C or 240 °C. The temperature was maintained at this set point for approximately 24 h and then the muffle furnace was turned off and the furnace and autoclave were allowed to cool for an additional 24 h. The contents of the autoclave were washed with 1.2 L of distilled water and then placed into a sonicated acid bath (0.1 N HCl) for 1 h. After acidification, the materials were washed with distilled water until they reached the natural pH of the distilled water (5.5–6). The washed nanomaterials were dried in an oven at 70 °C for 12 h and then calcined in a muffle furnace for 4 h at 550 °C or 700 °C. The synthesis conditions of the four nanomaterials used in this study are summarized in Table 2.

The temperatures used in the hydrothermal synthesis step and the calcination step were chosen based on the work of Yuan and Su [17], who observed that at a set reaction time and NaOH concentration (10 M) the hydrothermal temperature determined the size and shape of the products while the calcination temperature determined the crystal structure of the material. They observed that hydrothermal temperatures ranging from 100 °C to 180 °C resulted in the formation of cylindrical nanotubes while hydrothermal temperatures ranging from 180 °C to 250 °C yielded flatter nanoribbons/nanobelts. They also observed that materials calcined at 540 °C consisted primarily of TiO_2(B), a metastable form of TiO_2 while those calcined at temperatures above 700 °C for a short time consisted mainly of anatase, which is similar to the findings of other researchers [19].

Table 2
Summary of nanomaterial synthesis conditions and batch-to-batch consistency as determined by methylene blue dye degradation tests.

Nanomaterial	Hydrothermal Synthesis Temperature (°C)	Calcination Temperature (°C)	Average and Standard Deviation for Degradation of Methylene Blue Dye
P25	n/a	n/a	86 ± 1%
NB 130/550	130	550	37 ± 6%
NB 130/700	130	700	54 ± 1%
NB 240/550	240	550	41 ± 5%
NB 240/700	240	700	83 ± 1%

2.3. LENs quality control

Multiple batches of each nanomaterial were synthesized throughout this study. Before being used for experiments, each batch was evaluated for consistency based on its ability to degrade methylene blue dye. Quadruplicate samples containing 50 mL of 0.03 mM methylene blue solution dosed with 0.1 g/L of TiO_2 were stirred and exposed to UVA light (365 nm) with an average irradiance of 4.9 mW/cm^2 for 30 min (average UVA dose of 8.8 J/cm^2). A consistent pH of 5.5–6 was observed in each tested solution. The average results of these simple quality control tests are also presented in Table 2. Under the same experimental conditions P25 nanoparticles achieved 86 ± 1% decolourization of methylene blue.

2.4. Characterization of nanomaterials

The lab synthesized TiO_2 nanomaterials were characterized using transmission electron microscopy (TEM), selected area electron diffraction (SAED), available surface area (Brunauer–Emmett–Teller adsorption method), isoelectric point (IEP), and agglomerate size in distilled water and pre-filtered Otonabee River water.

TEM and SAED observation was conducted using a JEOL 2010F TEM/STEM at the Canadian Centre for Electron Microscopy (Hamilton, Ontario, Canada). TEM samples were prepared by drop casting the dispersions onto holey carbon grids. The images were processed using Gatan Microscopy Suite: Digial Micrograph™ and SAED and FFT images were indexed using CrysTBox – diffractGUI [25]. N_2 adsorption isotherms were measured with a Quantachrome AUTOSORB-1. The samples were outgassed at 200 °C under vacuum for 12 h before the measurement. Surface area was determined by BET method in a relative pressure range of 0.05–0.25.

The IEP of each engineered nanomaterial was determined by measuring its zeta potential at pH values ranging from 3 to 9. Zeta potential was measured using a Horiba Zeta Analyzer and all zeta potential experiments were conducted with 0.1 g/L of TiO_2 suspended in a 10 mM NaCl solution. The pH of the zeta potential samples was adjusted using 0.1 M NaOH or HCl. Two aliquots were analyzed from each sample.

A Malvern MasterSizer 3000 was used to evaluate the distribution size of the nanomaterial particles when prepared in distilled water and Otonabee River water. The latter was filtered through a 0.45 µm filter ahead of TiO_2 addition and measurement to avoid interference by natural particulate matter in the raw water. The background of each water matrix was evaluated before nanomaterial addition. Sufficient TiO_2 was then added to the water to achieve a 15% obscuration value. For all but one material, this obscuration value occurred at a TiO_2 concentration of approximately 0.03–0.06 g/L. NB 130/700 could not be analyzed under the same conditions as the other materials because its optical properties made it impossible to achieve the required obscuration at a concentration comparable to those used for the other materials. As a result, the size distribution data collected for NB 130/700 has not been included in this paper. Each sample was measured 10 times and the results were averaged and graphed as a volume distribution.

The formation of hydroxyl radicals by each of the nanomaterials was confirmed and quantified using the experimental apparatus described in Section 2.7 and a method adapted from Arlos et al. [26]. Distilled water was spiked with terephthalic acid (TPA), a probe compound that yields a fluorescent product (2-hydroxyterephthalic acid, HTPA) upon reaction with hydroxyl radicals. 50 mL samples containing 0.5 mM TPA dissolved in 6 mM NaOH were dosed with 0.02 g/L of TiO_2 and irradiated with UVA LED light for times ranging from 30 s to 15 min. The fluorescence of the samples was measured at an excitation wavelength of 315 nm and an emission wavelength of 425 nm. Dark controls (no irradiation) and light only (no TiO_2) controls were also prepared. In all cases no hydroxyl radical formation was observed in the control samples.

2.5. Settling tests

Aliquots of the 10 g/L TiO_2 stock solutions made with each nanomaterial were dispensed into an appropriate amount of distilled water or river water to create triplicate samples containing 250 mg/L (0.25 g/L) of TiO_2. The samples were sonicated for 5 min, transferred into the turbidimeter cuvette, and placed in the turbidimeter for a total of 2 h. The turbidity at midpoint of the cuvette was recorded at the beginning of the test and at 10 min intervals thereafter. The results of these simplified settling cannot be used to predict the long term behaviour of full-scale sedimentation basins, however, they do provide some indication of the relative settleability of the nanomaterials used in this study.

2.6. Measurement and characterization of natural organic matter

Raw and treated water samples were filtered through a 0.45 µm polyethersulfone (PES) laboratory filter before analysis. Natural organic matter was quantified as dissolved organic carbon (DOC) or based on UV absorbance at 254 nm (UV254). DOC was measured on an O/I Analytical Aurora 1030 TOC analyzer and UV254 was measured using an Agilent 8453 UV–vis spectrophotometer.

2.7. Dark adsorption and photocatalytic degradation under UVA light

The batch reactors were mixed using magnetic stir bars and irradiated with UVA LEDs (LZ1 UV 365 nm Gen2 Emitter, LED Engin Inc.) with a maximum irradiance at 365 nm and a rated power demand of 2.7 W. The irradiance of each lamp was confirmed before each test using a radiometer (International Light) optimized to measure light at 365 nm. A spreadsheet prepared by Bolton and Linden [27] was used to calculate the average irradiance of at the surface of the sample based on the irradiance measured at different points across the surface and the distance between the light source and the sample. The average irradiance at the surface of the samples was determined to be 4.9 mW/cm^2. All of the degradation experiments were conducted in quadruplicate at 0, 5, 15, 30, 45, and 60 min of irradiation. Samples were prepared in 75 mL batch reactors filled with 50 mL of raw river water obtained from a water treatment plant in Peterborough, Ontario, Canada and dosed with 0.25 g/L TiO_2. Light only controls were prepared by exposing samples of river water to UVA LED light for 60 min. Samples were analyzed for DOC and UV light absorbance at 254 nm (UV254).

2.8. Reusability of linear engineered nanomaterials

The reusability of two of the LENs, NB 130/550 and NB 240/700, was compared to that of P25 using a simplified version of the tests described in Section 2.7. In each case, 1.25 mL of 10 g/L TiO_2 stock solution was added to 50 mL of raw water and exposed to UVA LED light for 30 min. The TiO_2 was separated from the treated water via filtration, then resuspended in a fresh volume of raw water and once again exposed to UVA light for 30 min. Water samples from each treatment cycle were analyzed for UV254. This process was repeated a total of five times.

2.9. Electrical energy per order

The electrical energy per order (EEO) required to remove DOC and UV254 using P25 and each of the four LENs was calculated using the following equation:

$$EEO = \frac{1000Pt}{V\log\left(\frac{C_i}{C_f}\right)} \quad (1)$$

where P is the power dissipated by the treatment process (kW), V is the volume of water treated in the experiment (L), C_i is the original concentration of the contaminant, C_f is the final concentration of the contaminant, and t is the time required to achieve C_f (min).

3. Results and discussion

3.1. Nanomaterial Characterization

A summary of the physical and surface characteristics of the five nanomaterials employed in this study is provided in Table 3. As described in the subsequent subsections, the nanomaterials synthesized at 240 °C were larger and had fewer surface defects than those synthesized at 130 °C while the linear nanomaterials calcined at 550 °C contained both anatase and had higher IEPs and surface area than those calcined at 700 °C. The nanomaterials calcined at 700 °C were more photocatalytically active and produced more hydroxyl radicals than those calcined at 550 °C.

3.1.1. TEM

TEM images of the four engineered nanomaterials revealed differences in the shape and size of the nanomaterials formed under the different synthesis conditions (Fig. 1). As has been observed by others [17], the nanomaterials formed at the lower hydrothermal temperature (130 °C) were smaller in both length and width than those formed when the hydrothermal temperature was set at 240 °C. The materials calcined at 550 °C had rough, irregular surfaces while those calcined at 700 °C, irrespective of their geometry, had smooth but segmented surfaces. The former were similar to materials prepared by Zheng et al. [19], which were synthesized using a similar, though not identical method, and calcined at temperatures ranging from 550 °C to 650 °C. The authors attributed the irregular surfaces of their materials to the presence of TiO_2(B). Although the three dimensional shapes of the four nanomaterials were difficult to determine from the images, the NB 240/550 particles was flat or belt-like, matching the description of materials synthesized by Yuan and Su [17] and Zheng et al. [19] under similar conditions. Individual particles of NB 240/700 also appeared flat, but were irregularly shaped and occasionally segmented, perhaps indicating that particles that were originally rectangular in shape were in the process of being broken down during the high temperature calcination process.

3.1.2. SAED and HRTEM

SAED and HRTEM images of the four LENs are shown in Fig. 2. In all cases, crystal phase differed based on the temperature used in the calcination step. The crystalline structure of NB 130/550 belonged to the TiO_2(B) monoclinic system as indicated by the indexed SAED pattern (Fig. 2a1When the calcination temperature was increased to 700 °C as in NB 130/700, the crystal phase changed from TiO_2(B) to an anatase tetragonal system In Fig. 2c1, the SAED image of NB 240/550 was indexed as predominantly TiO_2(B) As with the samples hydrothermally synthesized at 130 °C, the samples hydrothermally synthesized at 240 °C exhibited the conversion of TiO_2(B) to anatase when increasing the calcination temperature from 550 °C to 700 °C as observed in Fig. 2d. This is in line with the findings of Zheng et al. [19], who found that TiO_2 LENs synthesized at 180 °C and calcined at 550 °C contained both anatase and TiO_2 while those calcined at 700 °C were pure anatase. Yuan and Su [17] had similar findings for LENs synthesized at 220 °C and calcined at 540 °C and 700 °C.

3.1.3. Surface area

The results of surface area testing (Table 3) show that hydrothermal temperature and calcination temperature both had effects on the BET surface area of the engineered nanomaterials. Surface area can impact adsorption efficiency and photocatalytic activity, though the latter is not a simple linear relationship [18]. In this study, lower temperatures during the hydrothermal and calcination steps were associated with higher BET surface area. Thus, NB 130/550 was found to have the highest surface area, the only one above that of P25 and at least double that of the other engineered nanomaterials, and NB 240/700 had the lowest. For the most part the BET surface area results for the LENs in this study presented in Table 3 compare favourably with results obtained by Qamar et al. [18] and Zheng et al. [19] for materials prepared under similar conditions. For example, Zheng et al. [19] synthesized TiO_2 LENs at 180 °C and calcined them at temperatures ranging from 300 °C to 700 °C. Their LENs had surface areas ranging from 16 m^2/g at 700 °C to 26 m^2/g at 300 °C, which is within the same range as the BET surface area of NB 240/700 (19 m^2/g), but below that of NB 240/550 (55 m^2/g). Similarly, LENs synthesized by Qamar et al. [18] at 150 °C and subsequently calcined at 700 °C had a BET surface area of 33 m^2/g, which is comparable to NB 130/700 in the current study (30 m^2/g). The LENs that Qamar et al. calcined at 500 °C had a surface area of 109 m^2/g, which is only slightly above that of NB 130/550 (99 m^2/g), and might be explained by the slightly lower temperature employed by Qamar et al. The lack of agreement between the results previous studies and the BET surface area of NB 240/550 in the current study may also be related to subtle differences in the synthesis and calcination temperatures and holding times employed in previous studies compared to the current one.

3.1.4. Isoelectric point

The isoelectric point of a substance can be determined by identifying the pH at which the zeta potential of a particle or colloid is zero. The zeta potential of the four engineered TiO_2 nanomaterials and that of P25 nanoparticles are shown in Fig. 3. Each point represents the average of four measurements made on a single aliquot by the zeta potential analyzer. The error bars represent the standard deviation of these four measurements. The estimated isoelectric point of each material based on the results presented in Fig. 3 is provided in Table 3.

The results indicate that calcination at 550 °C had no or only a small effect on the IEP of the engineered nanomaterials relative to their

Table 3
Characteristics of P25 and four linear engineered nanomaterials.

Nanomaterial	Crystal Phase(s)	BET Surface Area (m^2/g)	IEP	·OH Production Rate Constant (M/min)	Normalized ·OH Production Rate Constant ($M/min/m^2$)	R^2
P25	Anatase, Rutile	57	6.0–6.1	0.620 ± 0.029	0.870 ± 0.040	0.99
NB 130/550	Anatase, TiO_2(B)	99	6.0–6.1	0.127 ± 0.011	0.102 ± 0.009	0.97
NB 130/700	Anatase	30	4.2	0.312 ± 0.154	0.832 ± 0.412	0.97
NB 240/550	Anatase, TiO_2(B)	55	6.5	0.104 ± 0.009	0.151 ± 0.013	0.97
NB 240/700	Anatase	19	5.0	0.739 ± 0.058	3.110 ± 0.242	0.98

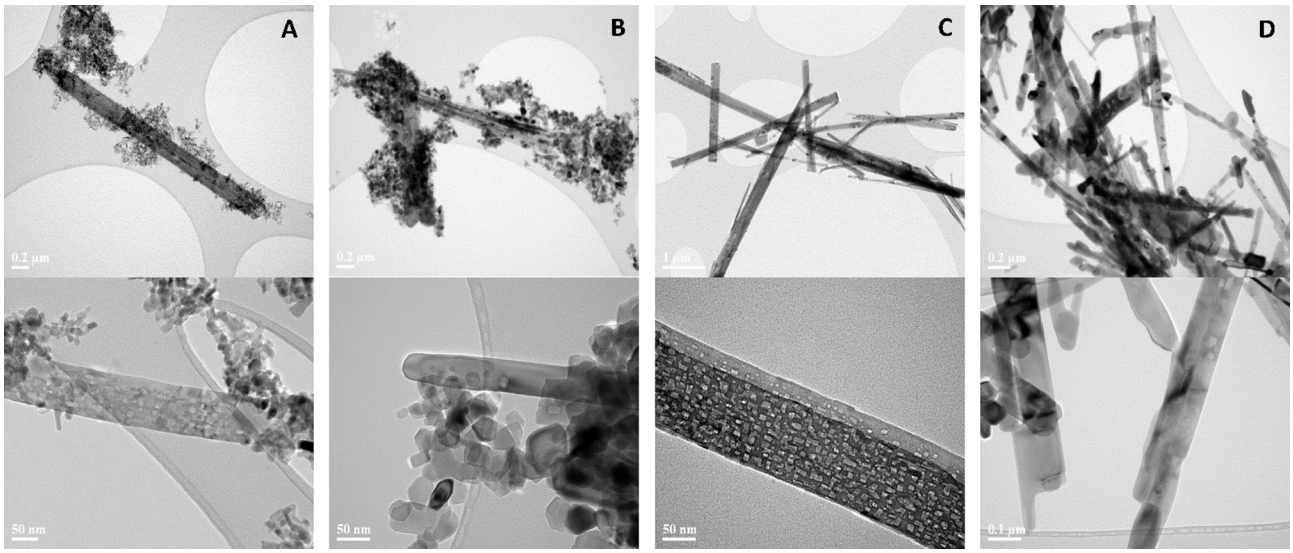

Fig. 1. TEM images of A: NB 130/550, B: NB 130/700, C: NB 240/550, D: NB 240/700.

precursor material (P25) but calcination at 700 °C decreased the IEP substantially, particularly for NB 130/700. These changes may have had an impact on the interactions between the engineered nanomaterials and the target contaminants in the raw water, particularly in terms of dark adsorption behaviour. The IEPs of the different materials would also be expected to have an effect on their agglomeration and settling behaviour in different water matrices because particles are generally more likely to agglomerate and settle when the pH of the water matrix is close to their IEP.

3.1.5. Hydroxyl radical formation

Fig. S1 shows the formation of HTPA via the reaction of TPA with hydroxyl radicals over time by P25 nanoparticles and the four LENs. Although it cannot be assumed that there was a one to one relationship between ·OH and HTPA formation – other researchers have assumed that only 80% of the ·OH formed during photocatalysis interact with TPA to form HTPA [28] – it can be assumed that the number of moles of ·OH formed was at least equal to the number of moles of HTPA formed. The materials calcined at 700 °C, which consisted primarily of anatase, produced far more HTPA, and thus ·OH radicals, than those calcined at 550 °C, which contained both anatase and TiO_2(B). While it is difficult to quantitatively compare the results of this study to those of other researchers because of differences in experiment apparatus and conditions (e.g. initial TPA concentration, TiO_2 dose, exposure time, irradiance, etc.), the results of the current study are within the same order of magnitude as those reported by other researchers using TiO_2 suspensions in batch reactors such as Turolla et al. [29].

As shown in Table 3, the rate of HTPA formation was an excellent fit (R^2 = 0.97–0.99) to a zero order reaction model. The rate of HTPA formation ranged from 0.104 ± 0.009 M/min for NB 240/550 to 0.739 ± 0.058 M/min for NB 240/700. When the reaction rate constants were normalized to the available surface area it was even more apparent that NB 240/700, which had a normalized reaction rate constant of 3.110 ± 0.242 M/min/m^2, was far superior to the other materials, which had normalized reaction rate constants ranging from 0.102 ± 0.009 M/min/m^2 for NB 130/550 to 0.870 ± 0.040 M/min/m^2 for P25, in terms of ·OH radical formation. Further discussion of these results is provided in Section 3.3.4.

3.2. Settling experiments and modeling

3.2.1. Results of settling tests

Conventional settling tanks in full scale water treatment plants are usually rectangular in shape, operate in a continuous flow through manner, and have detention times ranging from 1.5 to 4 h [30]. The standard bench-scale tests used to evaluate settling in water treatment applications, which require a relatively large volume of water, were not feasible for this study because of materials availability limitations. The simplified settling tests that were conducted instead clearly showed that the four engineered nanomaterials invariably settled more quickly than P25 (Fig. 4) in distilled water. NB 240/700 settled most quickly, followed by NB 130/550 and NB 240/550. The differences between these three materials were most apparent between 20 and 100 min. NB 130/700 was the slowest to settle and showed more variation between replicates than the other three engineered nanomaterials. An additional settling test was conducted to provide a qualitative visual counterpart to the data presented in Fig. 4. Photographs were taken of the materials at time zero and after 60 min and 24 h of settling (Fig. 5). The photographs clearly illustrate the superior settleability of the LENs compared to P25 nanoparticles in distilled water.

Nanomaterial synthesis conditions had a strong effect on settling efficiency. In general, the nanomaterials whose discrete particles appeared larger in the TEM pictures (NB 240/550 and NB 240/700) settled more effectively than the nanomaterials whose discrete particles appeared smaller. The particle size distributions of all of the nanomaterials except NB 130/700 are shown in Figs. S2 and S3. The “particles” detected by the particle sizer were larger than would be expected based on the TEM images of the nanomaterials, suggesting that they were agglomerates rather than discrete particles. The particle size distribution of NB 240/550 indicates that the solutions made with this material in both distilled water matrix and the river water matrix contained more large agglomerates than the suspensions made with the other engineered nanomaterials. The P25 particle size distribution skewed toward much smaller particle sizes than those of any of the engineered nanomaterials. All of the materials tested also varied in terms of their uniformity as indicated by the shape of their particle size distribution. The NB 240/550 agglomerates were the least uniform while those formed by P25 were the most uniform.

The results of the particle size distribution tests (Figs. S2 and S3) did not support the hypothesis that settling behaviour was exclusively a function of agglomerate size. Specifically, NB 240/550 formed he largest agglomerates, but this LEN settled out of the water more slowly than NB 130/550 or NB 240/700, both of which had size distributions that skewed toward smaller particle sizes. Other researchers have noted that the density of nanoparticle agglomerates is often lower than that of the constituent nanoparticles [31]. For example, Liu et al. [32]

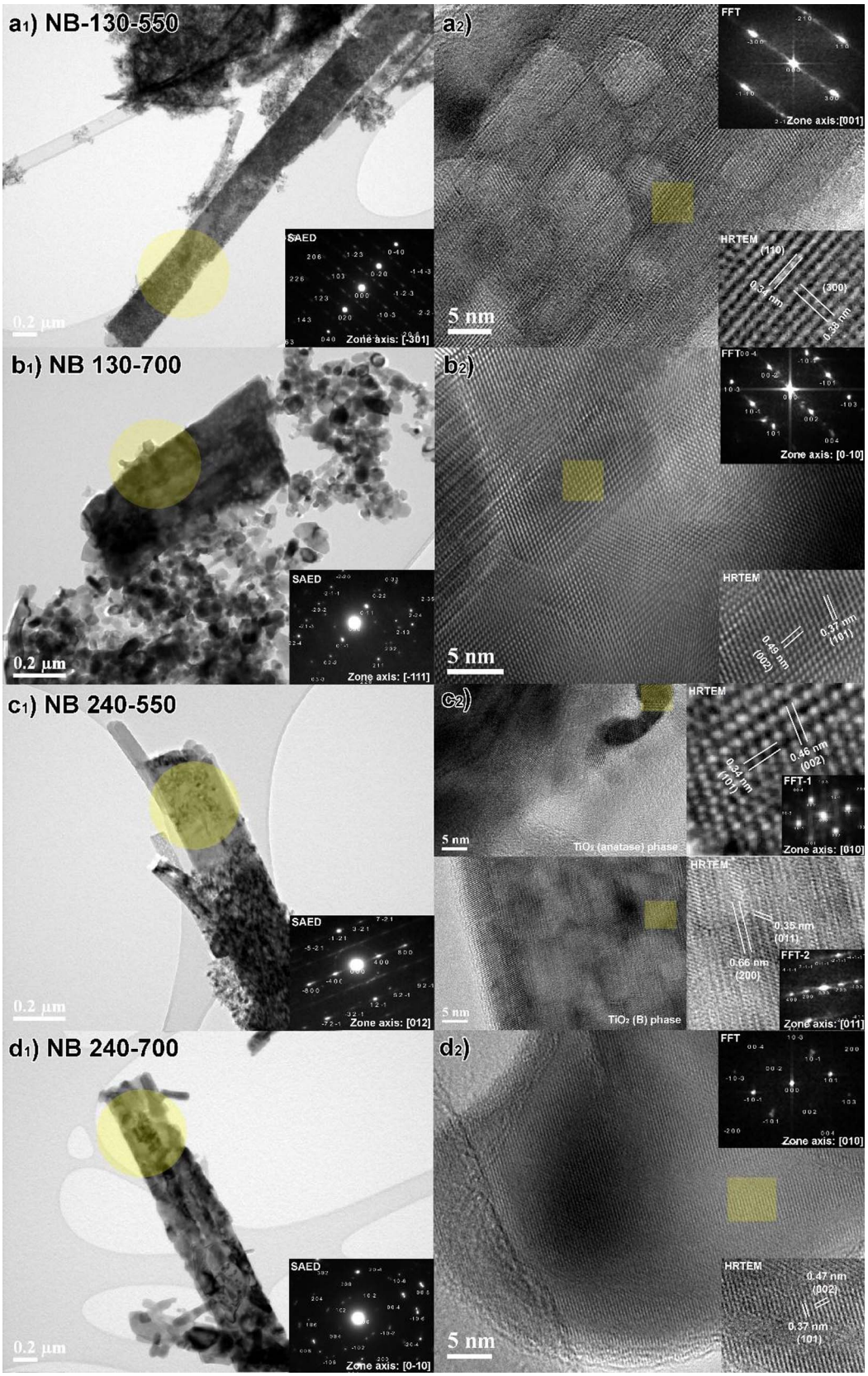

Fig. 2. HRTEM images with SAED indexed regions (yellow) and HRTEM images with corresponding FT image of NB samples. (For interpretation of the references to colour in this figure legend, the reader is referred to the web version of this article.)

determined that the effective density of the agglomerates formed by their linear engineered TiO_2 nanomaterials was 1.2 g/cm^3. Numerous factors can impact the effective density of the agglomerates formed by nanomaterials in solution including individual particle size, shape, and surface area [32,33]. For example, for linear TiO_2 nanomaterials, higher surface area has been linked to greater stabilization of

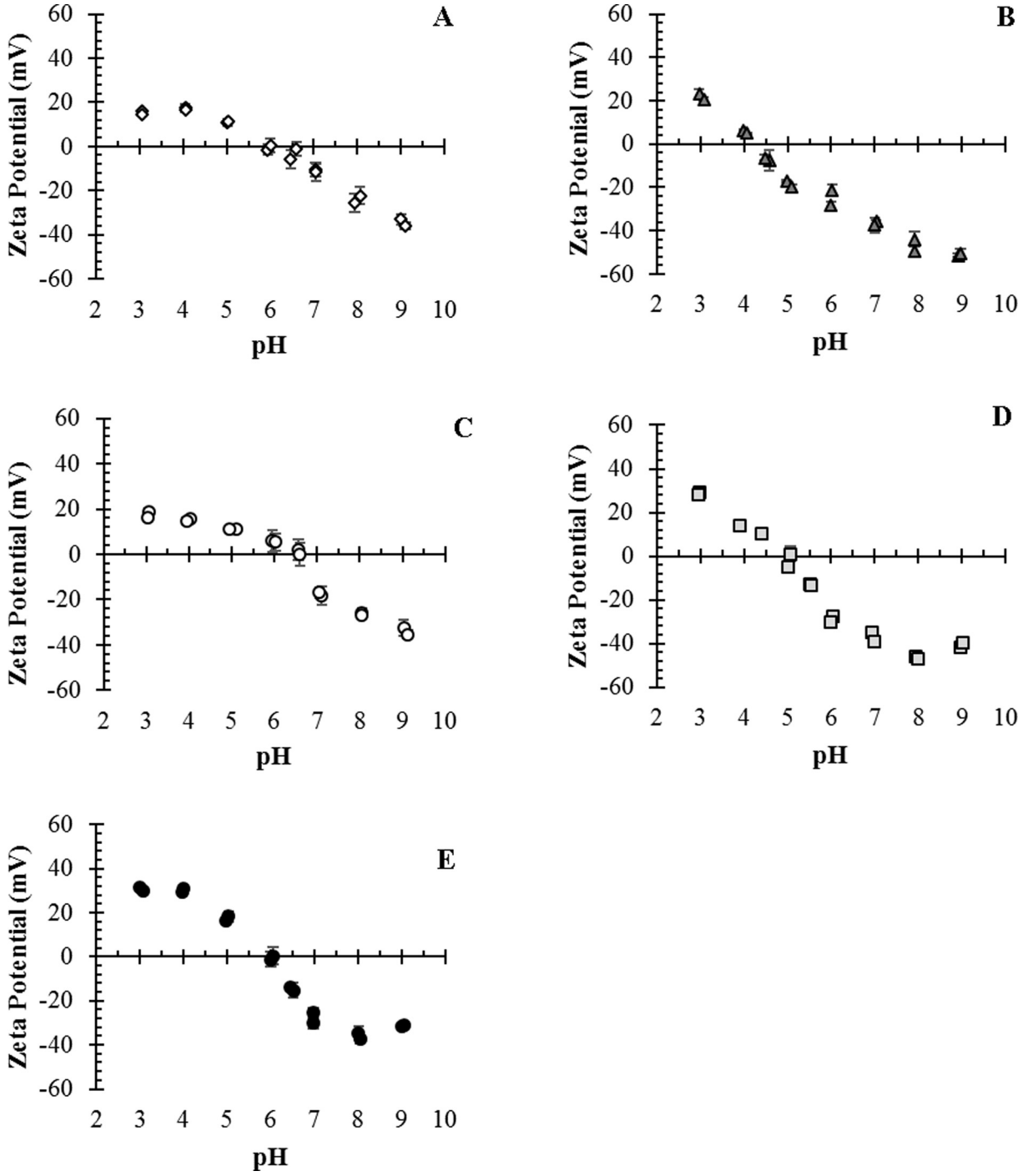

Fig. 3. Determination of isoelectric point of NB 130/550 (A), NB 130/700 (B), NB 240/550 (C), NB 240/700 (D), and P25 nanoparticles (E) using zeta potential at various pH conditions (two independent samples of each nanomaterial were analyzed by the instrument four times, error bars represent the standard deviation of all eight measurements).

nanomaterial suspensions. NB 240/550, which had a surface area of 55 m^2/g, did indeed settle more slowly than NB 240/700, which had a surface area of 19 m^2/g. The surface charge on the particles may also have impacted their settling efficiency because particles are more likely to agglomerate when the pH of the matrix is close to their IEP. The distilled water used in this study had a pH between 5.5 and 6. At this pH NB 130/550, NB 240/550, and NB 240/700 were all neutrally charged but NB 130/700 was negatively charged, making it more likely to remain dispersed in water. These phenomena alone do not explain the settling behaviour of NB 130/550, however, indicating that other forces may also have affected the agglomeration and settling of this nanomaterial in distilled water.

The settling tests were repeated in the Otonabee River water as shown in Fig. 4B. In this case, P25 nanoparticles actually settled more quickly than any of the engineered nanomaterials. This surprising finding may indicate the agglomerates formed by the P25 nanoparticles in this water matrix were larger or denser than those formed in the distilled water matrix. In contrast, the settling of the larger LENs (NB 240/550 and NB 240/700) was hindered in the river water matrix. This effect was less pronounced for the smaller LENs (NB 130/550 and NB 130/700). The settling behaviour observed in the river water was likely influenced by various components of the water matrix, particularly pH, NOM, and ions such as calcium, as well as the characteristics of the nanomaterials themselves. As described in the previous paragraph, pH

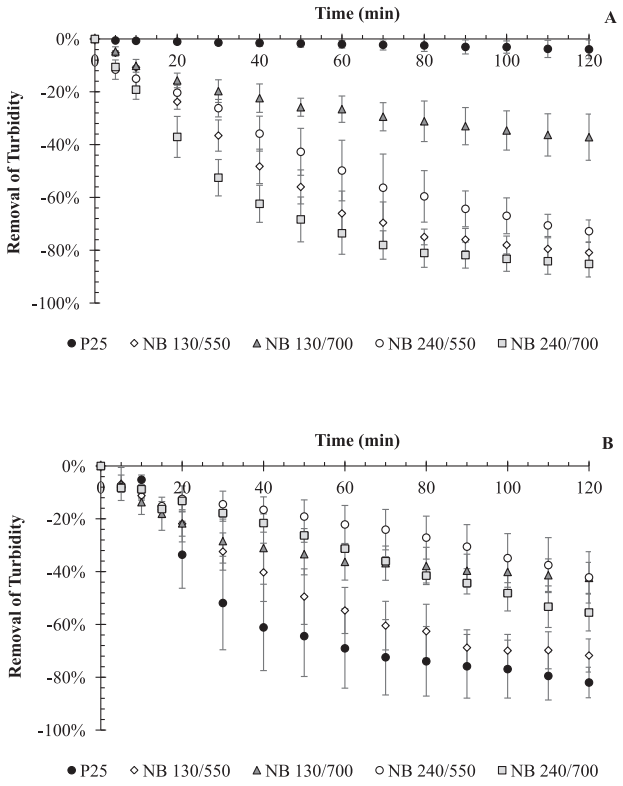

Fig. 4. Settling of P25 nanoparticles and four engineered nanomaterials in purified water and raw Otonabee River water (n = 3, error bars represent the standard deviation from the mean).

can influence the surface charge of the nanomaterial and thus its propensity to agglomerate. The pH of the river water was approximately 8, which is above the IEPs of all five nanomaterials used in this study. At this pH, the materials should all be less likely to agglomerate than at pH values closer to their IEPS (pH 4–6.5). Increasing levels of ions can minimize the repulsive electrostatic forces that keep particles from coming together, allowing van der Waals forces to dominate and encouraging greater agglomeration [33]. Additionally, the presence of calcium ions in the water matrix has been shown to increase the apparent IEP of TiO_2 nanomaterials as well as the size of their agglomerates and sedimentation efficiency [32,33], while humic acid (a major component of NOM) has been shown to have the opposite effects [32,34]. The size and shape of the nanomaterials can also impact their sedimentation efficiency because these material characteristics can influence the size and shape of the resulting agglomerates and the interactions of the materials with water matrix components [33]. For example, Liu et al. [32] showed that humic acid had a strong stabilizing effect on suspensions of linear TiO_2 nanomaterials but that the effect of ionic strength was dependent on the constituent ions and their concentration – in some cases, the addition of calcium actually stabilized the suspensions. Some or all of these phenomena may have influenced the results of the settling experiments presented in this study.

3.2.2. Modeling of settling results

Stokes' Law is commonly used to model the settling of discrete particles through a liquid medium. For a hard spherical particle, Stokes' Law can be simplified to:

$$v_s = \frac{g(\rho_p - \rho_w)d_p^2}{18\mu} \quad (2)$$

where v_s is the terminal settling velocity of the particle (m/s), g is the acceleration due to gravity (9.81 m/s^2), ρ_p is the density of the particle (kg/m^3), ρ_w is the density of the water (kg/m^3), d_p is the diameter of the particle (m), and μ is the viscosity of the water (kg/m.s).

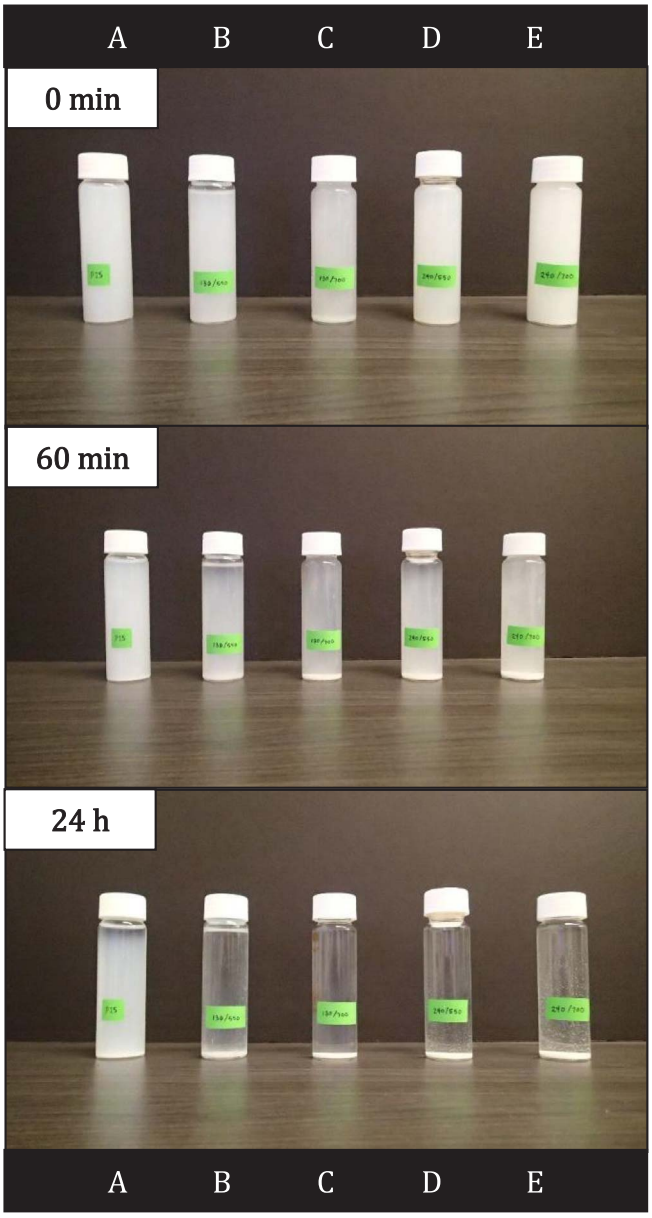

Fig. 5. Photographs of P25 (A), NB 130/550 (B), NB 130/700 (C), NB 240/550 (D), and NB 240/700 (E) settling in purified water.

The settling velocity predicted by Stokes' Law for P25 nanoparticles settling independently in solution was approximately six orders of magnitude slower than typical settling velocities for small and medium sized alum flocs as listed by Crittenden et al. [30] (Table S1). The settling velocities predicted for the LENs, which were calculated under the unrealistic assumption that the LENs or their agglomerates would behave as hard spheres, ranged from one to two orders of magnitude slower than typical values for alum flocs. If instead it was assumed that the various nanomaterials formed spherical agglomerates with hydrodynamic diameters equal to the D50 values obtained during the particle sizing tests, that the density of these agglomerates was equal to TiO_2's material density (4.26 g/cm^3), and that the agglomerates settled independently of one another, the settling velocities predicted for the four linear engineered nanomaterials ranged from 5.8×10^{-5} m/s for NB 130/550 in the river water matrix to 9.2×10^{-4} m/s for NB 240/550 in the distilled water matrix. The latter is within the range of typical settling velocities for small alum flocs provided by Crittenden et al.

[30]. Finally, if the effective density of the agglomerates was assumed to be equal to that reported by Liu et al. [32] for their LENs (1.2 g/cm^3), the settling velocities of the nanomaterials decreased by approximately one order of magnitude.

A sensitivity analysis was conducted to explore the effect of effective density on nanomaterial settling according to Stokes' Law. The results are presented in Table S6. Based on this analysis, it was determined that agglomerates of NB 130/550, NB 240/550, and NB 240/700 would have to have effective densities of 1.37 g/cm^3, 1.02 g/cm^3, and 1.21 g/cm^3, respectively, to conform to Stokes' Law in the distilled water and 1.44 g/cm^3, < 1.06 g/cm^3, and 1.16 g/cm^3 in the river water matrix. When these values were inputted into the Stokes' Law equation, the resulting predicted settling velocities ranged from 3.25×10^{-6} m/s for NB 240/550 in river water to 1.33×10^{-5} m/s for NB 240/700 in distilled water, which are approximately two orders of magnitude lower than typical values for alum flocs [30]. The same analysis suggested that P25 nanoparticles formed agglomerates in the river water matrix that were smaller in size but had a higher greater effective density (3.50 g/cm^3) than those formed by the LENs. This likely explains why the P25 nanoparticles settled more quickly than the LENs in the river water matrix.

This analysis suggests that the settling behaviour of the agglomerates of the P25 nanoparticles and the LENs could, to some extent, be modeled using Stokes' Law but also that the LENs settled more slowly than the particles formed during other common water treatment processes such as coagulation. The practical implication of this is that more and/or larger sedimentation tanks would be required for a system based around the LENs compared to one employing coagulation.

The calculations and results presented above are predicated on numerous assumptions, some of them better supported than others. In order to fully characterize the settling behaviour of the nanomaterials used in this study it would be necessary to know both the size and the effective density of the agglomerates formed by each material in the two water matrices. This was beyond the scope of this proof of concept study, however, it would be a necessary exercise if sedimentation were selected as the separation mechanism of choice in a TiO_2-based water treatment system.

3.3. Removal of DBP precursor surrogates via dark adsorption and photocatalytic degradation

3.3.1. DOC and UV254 removal by linear engineered nanomaterials

Under the experimental conditions used in this study, P25 nanoparticles removed 20% of the DOC (Fig. 6) and 31% of the UV254 (Fig. 7) present in the raw water through dark adsorption alone (i.e. at 0 min of irradiation). This is a substantial amount of removal given the relatively low concentration of TiO_2 employed in this study. The four engineered nanomaterials were less effective than P25 for DOC dark adsorption but all four nonetheless adsorbed at least a small amount. NB 130/550 and NB 240/550 were more adsorptive than the two materials calcined at 700 °C, likely owing to their greater surface area. Electrostatic attraction and repulsion effects may also have contributed to dark adsorption to some extent. Most NOM compounds are negatively charged above pH 4, thus in Otonabee River water, which has a pH of approximately 8, NOM would be negatively charged and the TiO_2 nanomaterials would either be neutral or negatively charged (NB 130/700 and NB 240/700). Electrostatic repulsion between negatively charged materials and negatively charged NOM may have prevented some adsorption that would otherwise take place due to other forces. This would explain why the materials calcined at 700 °C, which have lower IEPs and are negatively charged at ambient pH were less likely to adsorb NOM than P25 or the two nanomaterials calcined at 550 °C.

All four LENs were able to degrade DOC and UV254 to some extent as shown in Fig. 6 and Fig. 7. No removal of either parameter was observed in the light only controls (results not shown). P25 and NB 130/550 were the most effective for both DOC and UV254 removal,

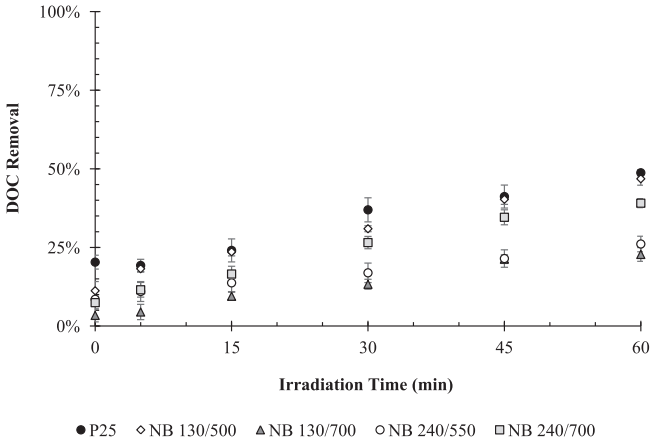

Fig. 6. Photocatalytic degradation of DOC by P25 nanoparticles and four engineered TiO_2 nanomaterials irradiated by UVA LED light (n = 4, error bars represent the standard deviation from the mean, no removal observed in light only controls).

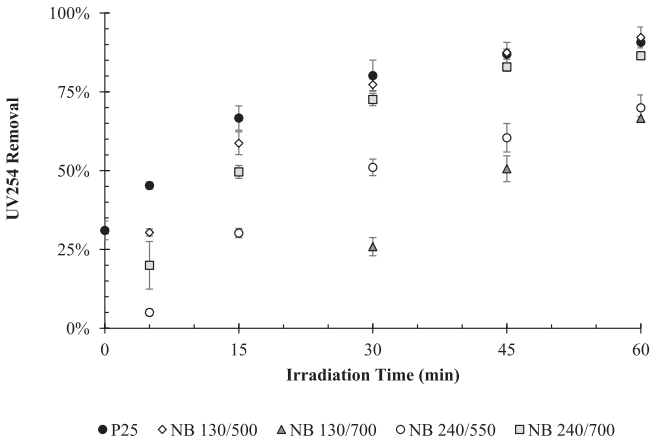

Fig. 7. Removal of UV254 by photocatalysis with P25 nanoparticles and four engineered TiO_2 nanomaterials irradiated by UVA LED light (n = 4, error bars represent the standard deviation from the mean, no removal observed in light only controls).

followed closely by NB 240/700. NB 240/550 and NB 130/700 were less effective but nonetheless removed over 25% of the DOC and approximately 70% of the UV254 in the raw water upon irradiation with UVA light.

For the most part, the degradation of DOC by P25 and the LENs fit a pseudo-first-order degradation model. The reaction rate constants (Table 4) followed the same trend as the removal values shown in Fig. 6 and Fig. 7, however, when the rate constants were normalized to the available surface area, a different pattern emerged. The materials calcined at 700 °C consistently had higher (1.5–3 times higher) normalized reaction rate constants than P25 and the two materials calcined at 550 °C, likely because the former consisted mainly of anatase and thus were more photocatalytically active and also because they produced more hydroxyl radicals upon irradiation. P25 and NB 130/550 nonetheless achieved good DOC and UV254 removal owing to their high surface area.

Our previous work and that of other researchers, though limited to P25 nanoparticles, has demonstrated that UV/TiO_2 photocatalysis degrades larger, more aromatic NOM compounds into smaller, less aromatic ones. This process has been linked to the formation of intermediate compounds that are more reactive with chlorine (and thus more likely to form DBPs when chlorine is added for disinfection) after short UV/TiO_2 treatment times followed by the gradual degradation of these intermediates at longer treatment times, with a resulting decrease in the overall DBPfp of the water [35,36]. The higher DOC and UV254 degradation rates observed for some of the LENs, especially after

Table 4
Reaction rate constants and R^2 values for the pseudo-first-order degradation of DOC by P25 nanoparticles and four engineered nanomaterials irradiated with UVA LED light (error values represent half of the 95% confidence interval of the rate constant).

Material	DOC			UV254		
	R^2	Rate constant, k (1/min)	Normalized rate constant, k_{norm} (1/min/m^2)	R^2	Rate constant, k (1/min)	Normalized rate constant, k_{norm} (1/min/m^2)
P25	0.93	−0.0034 ± 0.0004	−0.0048 ± 0.0006	0.96	−0.0146 ± 0.0013	−0.0205 ± 0.0019
NB 130/550	0.97	−0.0036 ± 0.0003	−0.0030 ± 0.0002	0.98	−0.0187 ± 0.0013	−0.0150 ± 0.0010
NB 130/700	0.93	−0.0017 ± 0.0002	−0.0046 ± 0.0005	0.99	−0.0142 ± 0.0007	−0.0378 ± 0.0017
NB 240/550	0.80	−0.0010 ± 0.0002	−0.0014 ± 0.0003	0.95	−0.0075 ± 0.0008	−0.0110 ± 0.0011
NB 240/700	0.97	−0.0031 ± 0.0002	−0.0131 ± 0.0010	0.96	−0.0155 ± 0.0015	−0.0653 ± 0.0062

normalization, suggests that these materials may be even more effective than P25 for DBPfp reduction. Specifically, NB 240/700 may prove to degrade DBP precursors more quickly and thus require less time to reach a point where overall DBPfp is decreasing, rather than increasing, and is the subject of ongoing research.

3.3.2. Reuse of LENs for NOM removal

Since NB 130/550 and NB 240/700 had been shown to be the most effective LENs for NOM removal (Figs. 6 and 7), reuse experiments were conducted with these two LENs and P25, the results of which are presented in Fig. 8. All three nanomaterials experienced significant ($p < .05$) decreases in treatment efficacy over successive reuse cycles, however, all three also retained some degree of photocatalytic activity even after 5 reuses. P25 experienced a sharp initial decrease in treatment efficacy after a single reuse (Fig. S4), while the reduction in treatment efficacy occurred more gradually for the two LENs. The result is that although P25 was initially more effective for NOM removal than the two LENs, after only a single reuse the LENs were able to reduce the UV254 of the water more effectively than the standard P25 nanoparticles. One possible explanation for this finding is that the agglomerates formed by P25, whether during treatment or during the filtration process used to remove the TiO_2 from the water after treatment, were tighter and less likely to break apart during resuspension, resulting in a decrease in available surface area and overall treatment ability. This is in line with the sedimentation modeling results (Table S6), which suggested that P25 nanoparticles would form small but dense agglomerates in the river water matrix while NB 130/550 and NB 240/700 would form larger, looser agglomerates. Further testing of the reusability of these materials would likely include a washing or regeneration step between uses. Many such cleaning processes are available today for similar materials, however testing each of them was clearly beyond the scope of the current study. In addition, since all of the experiments in this study were conducted in batch reactors, and the behaviour of the photocatalysts is unlikely to follow exactly the trends observed in this study if they were used in a flow through reactor, the impacts of flow regime would also be examined going forward. Nonetheless, the results presented here indicate that the two most promising LENs, NB 130/550 and NB 240/700, are comparable or superior to P25 nanoparticles in terms of reusability.

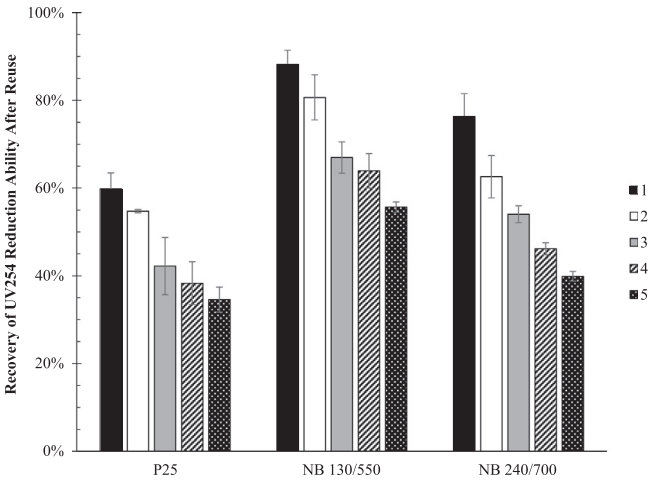

Fig. 8. Percent recovery of the UV254 reduction ability of P25, NB 130/550, and NB 240/700 after 1–5 reuses of the photocatalyst (n = 3, error bars represent the standard deviation from the mean).

3.3.3. Electrical energy per order for NOM degradation

The EEOs for DOC ranged from 242 kWh/order/m^3 for NB 130/550 to 1085 kWh/order/m^3 for NB 240/550 while those for UV254 ranged from 45 kWh/order/m^3 for NB 130/550 to 110 kWh/order/m^3 for NB 240/550. The EEOs followed the same trends as the first order reaction rate constants except that NB 130/550 had a slightly lower EEO for both parameters than P25, likely because the latter removed substantial amounts of DOC and UV254 via both dark adsorption and photocatalytic degradation and the EEO calculation only accounts for the photocatalytic portion of the treatment. Other researchers have reported similar EEO values for DOC removal from surface water using a pilot-scale UV/TiO_2 treatment system [37]. The EEO values calculated in the current study are above those reported by researchers using other AOPs. Yen and Yen [38] reported EEOs for DOC ranging from 12 kWh/order/m^3 to 30 kWh/order/m^3 using UV/H_2O_2 treatment. It should be noted, however, that this study employed a synthetic water matrix that contained commercial humic acid, which may not be as difficult to degrade as the complex mix of NOM in the Otonabee River water matrix, and unlike the Otonabee River matrix, did not contain any potential ROS scavengers such as bicarbonate or chloride [39] or any species such as calcium that might encourage nanoparticle agglomeration [32].

3.3.4. Comparison of reaction rate constants and implications for degradation pathways

The degradation rate constants and normalized degradation rate constants for DOC and UV254 were graphed against the formation rate constants for HTPA, a measure of ·OH radical formation (Table S7). There was no obvious correlation between the DOC or UV254 degradation rates and ·OH radical production rates, suggesting that not all of nanomaterials reduced these parameters via ·OH radical mediated reactions alone. There was a moderate correlation between the normalized DOC and UV254 degradation rates and ·OH radical production as predicted by HTPA formation. The correlation was much stronger if P25 removed from the analysis (Fig. S4). This indicates that the normalized DOC and UV254 degradation rates were good proxies for ·OH radical-related photocatalytic NOM degradation by the LENs but not for its photocatalytic degradation by P25. The fact that the correlation only existed when the NOM degradation rates were normalized to surface area suggests any additional NOM degradation observed for the LENs was related to surface phenomena such as oxidation by photo-generated electron holes. NOM degradation by P25 may have been more complex, possibly due to the formation of other ROS (e.g. superoxide) upon irradiation.

The practical implications of these differences on DBP precursor

removal are as of yet unclear, however, it may be that some LENs will be more likely than others to be negatively impacted by water matrix components such as ROS scavengers, which consume ·OH radicals and thus slow the overall rate of removal of target contaminants [38]. Additionally, species that compete with NOM for adsorption sites on the TiO_2 surface may decrease the effectiveness of LENs that operate primarily via surface mediated degradation reactions. Research to further characterize the mechanisms underlying NOM degradation by the different LENs is ongoing.

4. Conclusions

Four LENs were successfully synthesized using a simple hydrothermal method. The LENs differed from one another and from industry standard nanoparticles in terms of size, BET surface area, and other physical and chemical characteristics. The materials were all able to degrade substantial amounts of natural organic matter after less than an hour of irradiation with high intensity UVA LED light at 365 nm.

The materials varied in terms of their ability to reduce two disinfection byproduct precursor surrogates, DOC concentration and UV254 absorbance, but greater reductions were consistently observed for materials calcined at the higher temperature of 700 °C, particularly when the results were normalized to surface area. The variation was related to the surface area, charge, propensity to agglomerate, and crystal phase of the materials. The reaction rates were particularly influenced by the surface area and crystallinity of the materials. A simple fluorescence-based test was used to compare the nanomaterials in terms of their propensity to generate hydroxyl radicals when illuminated with UVA LED light. The results suggest that the predominantly anatase materials interacted with NOM primarily via hydroxyl radical mediated degradation reactions whereas the mixed phased nanomaterials removed NOM through a combination of adsorption and degradation reactions with photo-generated holes or ROS other than the ·OH radical.

All four engineered nanomaterials settled out from distilled water more quickly than standard P25 nanoparticles, likely due to their size and effective density of their agglomerates relative to those of P25 in this matrix. The results were reversed in a real river water sample – P25 settled out quickly, possibly due to the presence of agglomeration-inducing ions such as calcium in this water matrix, but the settling of the larger LENs was slightly hindered, likely due to the presence of NOM in the river water. Based on their ability to remove NOM and their reusability, a subset of these engineered nanomaterials may prove to be a viable alternative to P25 for drinking water treatment The settling results, however, suggest that despite their impressive settleability relative to P25 nanoparticles in distilled water, the applicability of the LENs as settleable photocatalysts may be limited in some real water matrices. This finding emphasizes the importance of site-specific testing for novel water treatment processes.

Acknowledgements

The authors would like to acknowledge the contributions of Leonardo Furtado, Jim Wang, Tassia Brito, Adrielle Costa, Wan-Ying (Jenny) Yue, Nathan Moore, Alireza Mahdavi, and Jeffrey Siegel to this project. Funding for this study was provided through Canada's Natural Sciences and Engineering Research Council's Strategic Project Grant program [STPGP 430654-12] and Canada Graduate Scholarship program as well as through the Ontario Graduate Scholarship program.

Appendix A. Supplementary data

Supplementary data associated with this article can be found, in the online version, at http://dx.doi.org/10.1016/j.cej.2017.10.058.

References

[1] Y. Nosaka, A.Y. Nosaka, Identification and roles of the active species generated on various catalysts, in: P. Pichat (Ed.), Photocatalysis and Water Purification: From Fundamentals to Recent Applications, Wiley-VCH Verlag GmbH and Co., 2013, pp. 1–24.
[2] A.-G. Rincón, C. Pulgarin, Bactericidal action of illuminated TiO_2 on pure *Escherichia coli* and natural bacterial consortia: post irradiation events in the dark and assessment of the effective disinfection time, Appl. Catal. B: Environ. 49 (2004) 99–112.
[3] T. Fotiou, T.M. Triantis, T. Kaloudis, A. Hiskia, Evaluation of the photocatalytic activity of TiO_2 based catalysts for the degradation and mineralization of cyanobacterial toxins and water off-odor compounds under UV-A, solar, and visible light, Chem. Eng. J. 261 (2015) 17–26.
[4] S. Liu, M. Lim, R. Fabris, C. Chow, K. Chiang, M. Drikas, R. Amal, Removal of humic acid using TiO_2 photocatalytic process – fractionation and molecular weight characterisation studies, Chemosphere 72 (2008) 263–271.
[5] K.K. Philippe, C. Hans, J. MacAdam, B. Jefferson, J. Hart, S.A. Parsons, Photocatalytic oxidation, GAC, and biotreatment combinations: an alternative for the coagulation of hydrophilic rich waters? Environ. Technol. 31 (2010) 1423–1434.
[6] D. Avisar, I. Horovitz, L. Lozzi, F. Ruggieri, M. Baker, M.-L. Abel, H. Mamane, Impact of water quality on removal of carbamazepine in natural waters by N-doped TiO_2 photo-catalytic thin film surfaces, J. Hazard. Mater. 244–245 (2013) 463–471.
[7] D. Kanakaraju, B.D. Glass, M. Oelgemoller, Titanium dioxide photocatalysis for pharmaceutical wastewater treatment, Environ. Chem. Lett. 12 (2014) 27–47.
[8] H. Shi, R. Magaye, V. Castranova, J. Zhao, Titanium dioxide nanoparticles: a review of current toxicological data, Part. Fibre Toxicol. 10 (2013) 15.
[9] Y. Yang, P. Westerhoff, Presence in, and release of, nanomaterials from consumer products, in: D.G. Capco, Y. Chen (Eds.), Nanomaterials, Advances in Experimental Medicine and Biology, Springer Science + Business Media, Berlin, 2014.
[10] T. Leshuk, P. Everett, H. Krishnakumar, K. Wong, S. Linley, F. Gu, Mesoporous magnetically recyclable photocatalysts for water treatment, J. Nanosci. Nanotechnol. 13 (2013) 3127–3132.
[11] M. Ng, E.T. Kho, S. Liu, M. Lim, R. Amal, Highly adsorptive and regenerative magnetic TiO_2 for natural organic matter (NOM) removal in water, Chem. Eng. J. 246 (2014) 196–203.
[12] S.-C. Kim, D.-K. Lee, Preparation of TiO_2-coated hollow glass beads and their application to the control of algal growth in eutrophic water, Microchem. J. 80 (2005) 227–232.
[13] N. Daneshvar, D. Salari, A. Niaei, M.H. Rasoulifard, A.R. Khataee, Immobilization of TiO_2 nanopowder on glass beads for the photocatalytic decolorization of an azo dye C.I. Direct Red 23, J. Environ. Sci. Health 40 (2005) 1605–1617.
[14] S. Liu, M. Lim, R. Amal, TiO_2-coated natural zeolite: rapid humic acid adsorption and effective photocatalytic regeneration, Chem. Eng. Sci. 105 (2014) 46–52.
[15] T. Kasuga, M. Hiramatsu, A. Hoson, T. Sekino, K. Niihara, Titania nanotubes prepared by chemical processing, Adv. Mater. 11 (1999) 1307–1311.
[16] C.L. Wong, Y.N. Tan, A.R. Mohamed, A review on the formation of titania nanotube photocatalysts by hydrothermal treatment, J. Environ. Manage. 92 (2011) 1669–1680.
[17] Z.-Y. Yuan, B.-L. Su, Titanium oxide nanotubes, nanofibres, and nanowires, Colloids Surf. A: Physicochem. Eng. Aspects 241 (2004) 173–183.
[18] M. Qamar, C.R. Yoon, H.J. Oh, N.H. Lee, K. Park, D.H. Kim, K. Lee, W.J. Lee, S.J. Kim, Preparation and photocatalytic activity of nanotubes obtained from titanium dioxide, Catal. Today 131 (2008) 3–14.
[19] Z. Zheng, H. Liu, J. Ye, J. Zhao, E.R. Waclawik, H. Zhu, Structure and contribution to photocatalytic activity of the interfaces in nanofibers with mixed anatase and TiO_2(B) phases, J. Mol. Catal. A: Chem. 316 (2010) 75–82.
[20] S. Hrudey, Chlorination disinfection by-products, public health risk tradeoffs, and me, Water Res. 43 (2009) 2057–2092.
[21] S. Krasner, The formation and control of emerging disinfection by-products of health concern, Philos. Trans. R. Soc. 367 (2009) 4077–4095.
[22] D. Zheng, R.C. Andrews, S.A. Andrews, L. Taylor-Edmonds, Effects of coagulation on the removal of natural organic matter, genotoxicity, and precursors to halogenated furanones, Water Res. 70 (2015) 118–129.
[23] J. van Leeuwen, R. Daly, R. Holmes, Modeling the treatment of drinking water to maximize dissolved organic matter removal and minimize disinfection by-product formation, Desalination 176 (2005) 81–89.
[24] A.D. Pifer, J.L. Fairey, Suitability of organic matter surrogates to predict trihalomethane formation in drinking water sources, Environ. Eng. Sci. 31 (2014) 117–126.
[25] M. Klinger, A. Jäger, Crystallographic Tool Box (CrysTBox): automated tools for transmission electron microscopists and crystallographers, J. Appl. Crystallogr. 48 (2015), http://dx.doi.org/10.1107/S1600576715017252.
[26] M. Arlos, R. Liang, M. Hatat-Fraile, L. Bragg, N.Y. Zhou, M. Servos, S. Andrews, Photocatalytic decomposition of selected estrogens and their estrogenic activity by UV-LED irradiated TiO_2 immobilized on porous titanium sheets via thermal-chemical oxidation, J. Hazard. Mater. 318 (2016) 541–550.
[27] J.R. Bolton, K.G. Linden, Standardization of methods for fluence (UV dose) determination in bench-scale UV experiments, J. Environ. Eng. 129 (2003) 209–215.
[28] K. Ishibashi, A. Fujishima, T. Watanabe, K. Hashimoto, Quantum yields of active oxidative species formed on TiO_2 photocatalyst, J. Photochem. Photobiol. A: Chem. 134 (2000) 139–142.
[29] A. Turolla, A. Piazzoli, J.F. Budarz, M.R. Wiesner, M. Antonelli, Experimental measurement and modeling of reactive species generation in TiO_2 nanoparticle

photocatalysis, Chem. Eng. J. 271 (2015) 260–268.
[30] J.C. Crittenden, R.R. Trussell, D.W. Hand, K.J. Howe, G. Tchobanoglous, MWH's Water Treatment: Principles and Design, 3rd ed., John Wiley and Sons, 2012.
[31] G. Deloid, J.M. Cohen, T. Darrah, R. Derk, L. Rojanasakul, G. Pyrgiotakis, W. Wohlleben, P. Demokritou, Estimating the effective density of engineered nanomaterials for in vitro dosimetry, Nat. Commun. 5 (2014) 3514, http://dx.doi.org/10.1038/ncomms4514.
[32] W. Liu, W. Sun, A.G.L. Borthwick, J. Ni, Comparison on aggregation and sedimentation of titanium dioxide, titanate nanotubes, and titanate nanotubes-TiO_2: influence of pH, ionic strength, and natural organic matter, Colloids Surf. A: Physicochem. Eng.Aspects 434 (2013) 319–328.
[33] E.M. Hotze, T. Phenrat, G.V. Lowry, Nanoparticle aggregation: challenges to understanding transport and reactivity, J. Environ. Qual. 39 (2010) 1909–1924.
[34] B.J.T. Thio, D. Zhou, A. Keller, Influence of natural organic matter on the aggregation and deposition of titanium dioxide nanoparticles, J. Hazard. Mater. 189 (2011) 556–563.
[35] S. Gora, S. Andrews, Adsorption of natural organic matter and disinfection byproduct precursors from surface water onto TiO_2 nanoparticles: pH effects, isotherm modelling and implications for using TiO_2 for drinking water treatment, Chemosphere 174 (2017) 363–370.
[36] S. Liu, M. Lim, R. Fabris, C.W.K. Chow, M. Drikas, G. Korshin, R. Amal, Multi-wavelength spectroscopic and chromatography study on the photocatalytic oxidation of natural organic matter, Water Res. 44 (2010) 2525–2532.
[37] D. Gerrity, B. Mayer, H. Ryu, J. Crittenden, M. Abbaszadegan, A comparison of pilot-scale photocatalysis and enhanced coagulation for disinfection byproduct mitigation, Water Res. 43 (2009) 1597–1610.
[38] H.Y. Yen, L.S. Yen, Reducing THMfp by H_2O_2/UV oxidation for humic acid of small molecular weight, Environ. Technol. 36 (4) (2015) 417–423.
[39] C.-H. Liao, S.-F. Kang, F.-A. Wu, Hydroxyl radical scavenging role of chloride and bicarbonate ions in the H_2O_2/UV process, Chemosphere 44 (2010) 1193–1200.